Simulations of a grazing-incidence pumped x-ray laser at 14.7 nm

F. Yan, J. Zhang,* Q. L. Dong, and X. Lu

Laboratory of Optical Physics, Institute of Physics, Chinese Academy of Sciences, Beijing 10080, China

Y. J. Li

Department of Physics, China University of Mining & Technology (Beijing), Beijing 100083, China

Numerical simulations of the grazing-incidence pumped Ni-like Pd x-ray laser at 14.7 nm ($4d \rightarrow 4p$, $J=0 \rightarrow 1$) is performed using a modified one-dimensional hydrodynamic code MEDUSA. The effective absorption of the main laser pulse in the gain region is greatly increased due to the lengthened propagation path. Results predict that a saturated output of the x-ray laser can be achieved with only subjoules driver energy on a 4-mm-long Pd target.

PACS number(s): 42.55.Vc, 32.30.Rj, 42.60.By, 52.50.Jm

I. INTRODUCTION

Since a demonstration of amplification of collisionally pumped x-ray lasers in 1984 [1], great efforts have been devoted into the development of compact high-repetition-rate x-ray lasers operating in saturation regimes and capable of delivering sufficient average output powers for various applications. The most important task to reach such a goal is to improve the coupling efficiency of the pumping driver energy into the x-ray laser energy. With the application of the prepulse technique [2], the required pumping energy has been reduced from kilojoules to hundreds of joules to achieve saturation operations of x-ray lasers at wavelengths as short as 5.8 nm [3–6]. A transient collisional excitation (TCE) scheme [7] was also used to improve the efficiency, where a subnanosecond laser pulse produces a preplasma abundant of Ne-like or Ni-like ions; a short main laser pulse then rapidly heats the plasma to a level high enough to generate the transient population inversion. An optimized delay time is usually introduced between the two successive pulses to generate a smooth electron density profile. With the TCE scheme, the drive energy necessary for a saturated operation of a x-ray laser at wavelengths longer than 15 nm has been further reduced to several joules [8–15].

However, the coupling of the drive energy into the gain region is not very efficient. At the normal incidence of the laser pulses, the drive energy is mainly absorbed near the critical surface via the resonance absorption, only a little part is absorbed via the inverse bremsstrahlung (IB) absorption in the useful gain region. To avoid the deleterious resonant absorption and to improve the drive efficiency, a longitudinal pumping scheme was proposed with the main laser pulse incident along the axis of the preformed plasma column. The Ni-like Mo x-ray laser at 18.9 nm longitudinally pumped by a laser energy of only 150 mJ was demonstrated to lase [16] yet not in saturation operation, because of the nonuniform heating of the gain medium region due to the significant drive energy loss by further ionization and excitation processes along the laser path.

Recently the grazing incidence pumping (GRIP) scheme, proposed by Dunn *et al.*, as a promising scheme for efficient x-ray lasers operating at a high repetition rate with a middle-Z target [17,18]. The GRIP scheme, which in principal is a TCE one, still utilizes a two-step-pumping arrangement, with a prepulse at normal incidence onto a slab target to produce the plasma column, while a short main laser pulse incident at a determined grazing incidence angle on the preformed plasma to generate the population inversion. Figure 1 sketches the geometry. The grazing incidence angle can be determined by the location of the suitable plasma electron density region chosen for selected atomic kinetics to realize an x-ray laser at a specific wavelength. The GRIP arrangement allows the controlled use of the refraction of the pumping laser pulse. This brings about several benefits. The length of the gain medium, produced by the simple optics geometry, is limited only by the diameter of the pumping laser beam itself [19]. The grazing incidence of the main pulse ensures more uniform heating of the preformed plasma column in the fact that different parts in the cross section of the laser pulse irradiate different parts of the plasma along the axis in successive order, which overcomes defects of the longitudinal pumping arrangement discussed above [16]. The effective absorption of the pumping pulse by the preformed plasma is enhanced by 3–10 times due to the lengthened propagation path in the gain region. This is advantageous for the gain achievement with the pumping applying short pulses of sub-joules. The GRIP scheme also realizes an inherent traveling
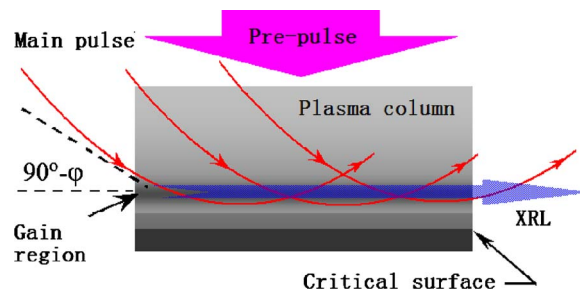
FIG. 1. (Color online) Sketch of the grazing incidence pumping scheme.

*Email address: jzhang@aphy.iphy.ac.cn

wave pumping, whose speed is determined by the grazing incidence angle and slightly smaller than *c*. A grazing incidence pumped Ni-like Mo x-ray laser operation at 18.9 nm was demonstrated [18] using a total energy of 150 mJ in the prepulse and the main pulse.

In this paper the operation of the Ni-like Pd x-ray laser at 14.7 nm $(4d \rightarrow 4p, J=0 \rightarrow 1)$ driven by subjoule laser pulses applying the grazing incidence scheme is numerically investigated using a modified one-dimensional hydrodynamic code MEDUSA [20] coupled with an atomic code. Note that several groups have demonstrated lasing in soft x-rays of different wavelengths [21,22]. Those x-ray lasers, all based on the same atomic system, have saturated or nearly saturated output yet in different regimes. This is because the pumping laser systems vary in experiments of different laboratories, and parameter flexibilities of a single laser set are far from sufficient to scan the full range of interests. Numerical simulation is then the study method usually adopted for explanation of the variation of operating regimes and to perform optimizations of driving laser configurations of specific systems. The present work reproduces the saturated Mo x-ray laser of 18.9 nm with one set of optimized experimental conditions [18] and designs other x-ray lasers with the pumping laser systems of different parameters. Detailed simulations were performed to optimize the driving laser configurations. The Ni-like Pd x-ray laser at 14.7 nm is predicted to saturate with drive energy of only hundreds of millijoules on 4-mm-long slab targets.

II. MODEL DESCRIPTION

The numerical simulations of the x-ray lasers were carried out with the hydrodynamic code MEDUSA coupled with an atomic package. MEDUSA is a one-dimensional Lagrangian hydrodynamic code, which was used to simulate the laser-plasma interaction. However, the code was only capable of the normal incidence. Modifications were carried out for the investigation of the grazing incidence pumping scheme.

The situation of the short main laser pulse is approximated as a plane electromagnetic wave incident onto the preformed plasma column with an electron density $n_e(x)$. The vacuum-plasma interface is located at $x=0$. The incidence angle φ is defined as the angle between the laser propagation vector and the direction of electron density gradient. Without loss of generality, the incidence plane is taken to be the *X-Z* plane, as shown in Fig. 2(a). In this case, the reflection of the light wave occurs at n_e where $\sin^2 \varphi = 1 - n_e/n_c$ [20], with n_e as the electron density at the turning point of the main laser beam, and n_c the critical density corresponding to the pumping laser wavelength.

Absorption is assumed to occur via the inverse Bremsstrahlung in the region with a density ρ below the critical density $\rho_c = (\varepsilon_0 M m_H m_e / Z e^2) \omega_L^2$ kg/m³, where the plasma frequency equals the frequency ω_L of the laser light. The absorption coefficient of the inverse bremsstrahlung is given by [19]

$$\alpha = 13.51 \lambda^{-2} \beta^2 (1-\beta)^{-1/2} T_e^{-3/2} \times (5.05 + \log \lambda T_e) \overline{Z^2} \text{ m}^{-1} \tag{1}$$
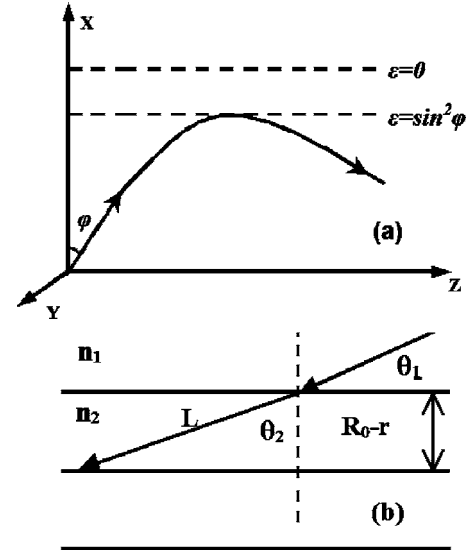
FIG. 2. Sketch illustrating a light ray obliquely incident onto a plasma slab.

where $\beta = \rho/\rho_c < 1$ and λ is the wavelength of the pumping laser beam. Assuming $P_L(R_0)$ is the laser power incident on the plasma boundary at $r=R_0$, then

$$P_L(r,t) = \exp[-\alpha(R_0 - r)] P_L(R_0,t). \tag{2}$$

The equation of the main short laser beam propagating in the plasma is described with a ray path partitioned into *N* intervals $[r_{i-1}, r_i]$ of length *L*, as shown in Fig. 2(b). The grazing incidence pulse suffers refraction in the plasma due to the electron density gradient. Assuming the main pulse beam propagating from a plasma region with a refraction index n_1 into a region with a refraction index n_2, we have $n_1 \sin \theta_1 = n_2 \sin \theta_2$. So the length *L* can be expressed by $L=(R_0-r)/\cos \theta_2$, where θ_1 and θ_2 are the angles of incidence and refraction, respectively. The propagation path of the pumping laser beam in the plasma is lengthened when the pumping pulse beam varies from the normal incidence to the grazing incidence, which results in the great IB absorption enhancements in the region before the turning point.

III. EXPERIMENT REPRODUCTION

As verification of the modified hydrodynamic code, we reproduced the experiments with GRIP arrangements [18]. The experiments had a 200 ps prepulse of 5×10^{11} W/cm² launched 500 ps before the 1.5 ps main short pulse of 4×10^{13} W/cm². With a total driving energy of 150 mJ, the Ni-like Mo x-ray laser at 18.9 nm was demonstrated to operate near saturation with an achieved gain-length product of 14 for a 4 mm target length, as shown by dots in Fig. 3. A good agreement between the simulation and the experimental results is found. Detailed simulation results are shown in Fig. 4, indicating the advantages of the GRIP arrangements.

Figure 4 gives the electron density (a), electron temperature (b), and absorbed laser power density (c) profiles from the grazing incidence pumping scheme and the normal incidence pumping scheme, respectively. The shadow area rep-
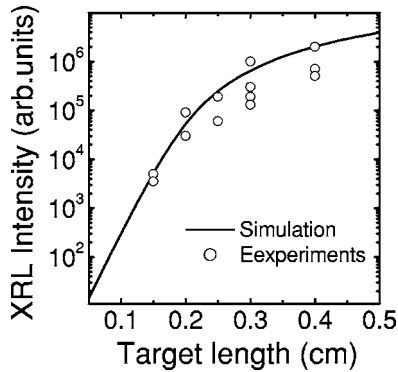
FIG. 3. Spatially integrated x-ray laser output intensity as a function of the plasma column length for simulations of experiments [18].

resents the gain region. The grazing incidence angle for the Ni-like Mo x-ray laser at 18.9 nm is 13.8°. The corresponding electron density at the turning point is about 10^{20} cm^{-3}. Figure 4(a) indicates that the x-ray laser beam is emitted at an electron density of $3-5 \times 10^{19}$ cm^{-3} and up to a maximum of 10^{20} cm^{-3}. This agrees with the expected electron density in Ref. [18]. For the normal incidence scheme, the highest electron temperature T_e of 150 eV locates near the critical electron density, while T_e is only 50 eV in the gain
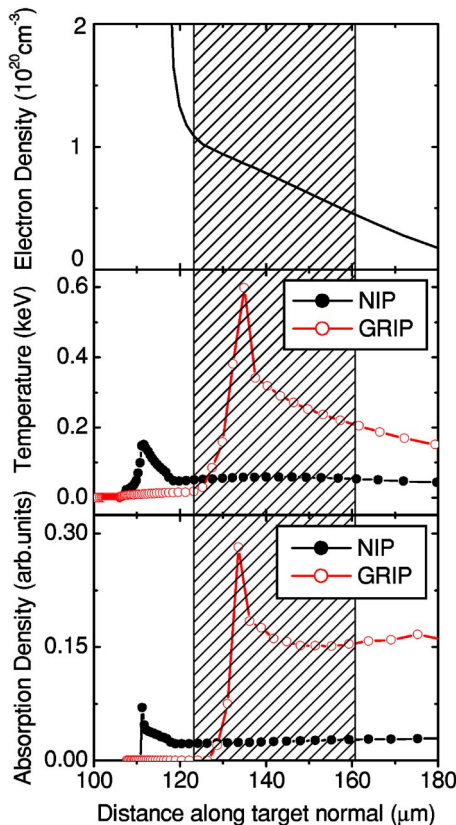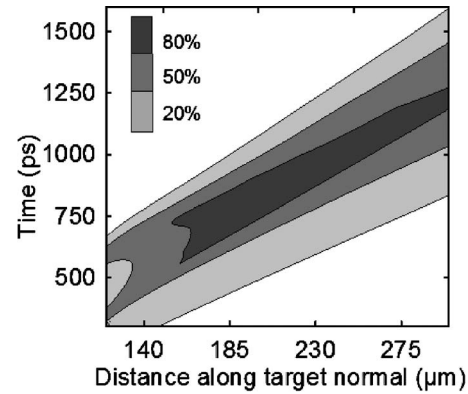
FIG. 5. Contours of the Ni-like Pd ion abundance versus space and time. The color from light to dark represents the Ni-like ion abundance over 20%, 50%, and 80%, respectively.

region. The highest T_e can reach 520 eV in the gain region for the GRIP scheme due to the greatly increased absorption density in the selectable media region, as shown in Fig. 4(c). The simulation results reproduce the experimental results of the plasma media in Ref. [18] and result in a good agreement.

IV. THE SIMULATION OF THE PD X-RAY LASER AT 14.7 NM

In this section we show the optimization of the driving configuration with about 600 mJ energy for a saturated operation of the Ni-like Pd x-ray laser at 14.7 nm. In the following simulation, a Gaussian pulse profile at 800 nm and a 100-μm-thick slab Pd target are used.

First, we carried out the optimization of the prepulse. Since the duration of the uncompressed laser pulse is fixed at 300 ps, we mainly optimize the pulse intensity. Figure 5 shows the contours of the spatial and temporal evolution of the Ni-like ion abundance in the plasma formed by the prepulse with a peak intensity at 1.2×10^{12} W/cm^2. The target surface is located on the figure at 100 μm and the pumping pulse reaches its peak intensity at 360 ps. The color from the light to the dark represents the Ni-like ion abundance over 20%, 50%, and 80%, respectively. In the optimization, we deliberately used a higher peak intensity of the prepulse to induce a little overionization in the preformed plasma with high Ni-like ion abundance. Such arrangement results in a higher electron temperature, preventing decrease of the Ni-like ion population via electron-ion recombination due to longer delays between the prepulse and the main pulse and generating more smooth electron density profile.

The temporal delay between the two pumping pulses is of fundamental importance to x-ray laser performance as in the transverse pumping scheme because it determines the state of the plasma column, which in turn affects dramatically the

FIG. 4. (Color online) Details of the simulation for experiments in [18]. Figure shows electron density (a), electron temperature (b), and absorbed laser power density (c) versus space for the grazing-incidence pumping scheme and the normal-incidence pumping scheme, respectively. The shadow represents the gain region.

propagation and absorption of the main pulse. Figure 6 gives the spatial and temporal distribution of the electron density produced by the prepulse. The optimum electron density for the Ni-like Pd x-ray laser of 14.7 nm is about 1×10^{20} cm^{-3} [23]. In combination with the requirements of
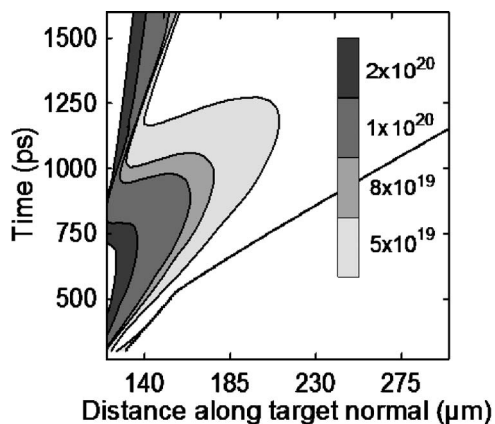
FIG. 6. Contours of the electron density versus space and time. The color from light to dark represents the electron density over 5×10^{19}, 8×10^{19}, 1×10^{20}, and 2×10^{20} cm^{-3}, respectively.

the electron density and Ni-like Pd ion population distribution as shown in Fig. 5, the turning point of the main pulse at grazing incidence is determined at 3×10^{20} cm^{-3}, while the optimum time to launch the main pulse is determined between 800 and 900 ps, and from 450 to 550 ps after the peak of the preforming pulse. Before this time range, the electron density gradient is too steep for the x-ray laser propagation. On the other side, both of the electron temperature and the Ni-like Pd ion population decrease if the main pulse is launched too late. This will in turn increases the requirement for the main pulse energy. The existence of such a narrow temporal lasing window indicates the sensitive dependence of the x-ray laser performance on the driving pulse configuration demanding.

Figure 7 gives the detailed simulation results at the peak of the main pulse. The electron temperatures in the grazing-incidence pumping scheme and the normal-incidence pumping scheme are compared. It shows that for the normal incidence the pumping laser energy is mainly absorbed near the critical density surface of 10^{21} cm^{-3} but not in the gain region of 10^{20} cm^{-3}, and the highest electron temperature is only around 300 eV. The grazing incidence has much higher coupling efficiency of energy into the 10^{20} cm^{-3} density re-
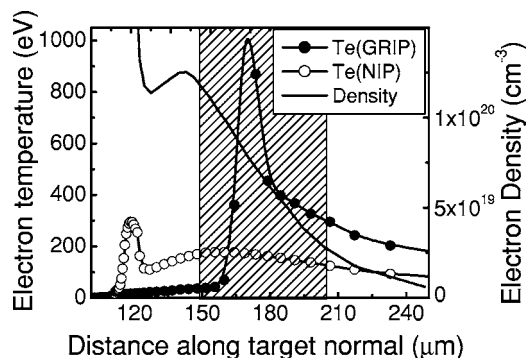
FIG. 7. Comparisons of the electron temperature between the grazing-incidence pumping scheme (GRIP) and the normal-incidence pumping scheme (NIP) for Ni-like *Pd* 14.7 nm x-ray laser system. The shadow represents the local gain region. The solid line is the electron density profile.
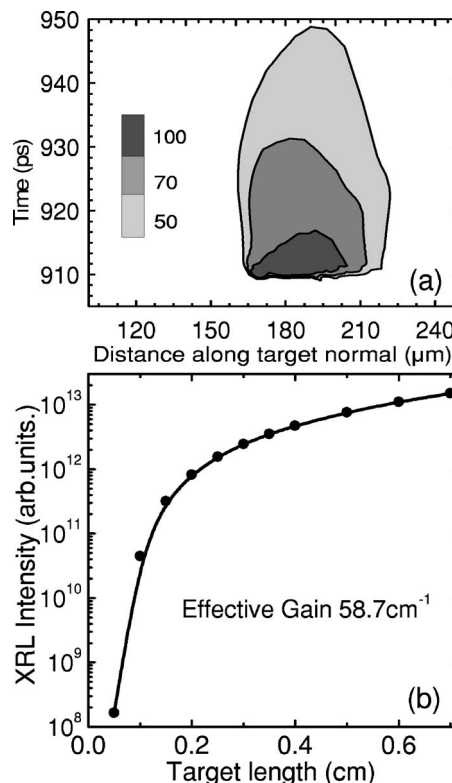
FIG. 8. Contours of the gain vs space produced by the main pulse of 1 ps with a peak intensity of 2×10^{14} W/cm^2 (a). (b) shows the spatially integrated x-ray laser intensity as a function of the plasma column length.

gion and shows electron temperature of about 1000 eV because of the enhancement of absorption. The shadow in the figure represents the local gain region. The solid line is the electron density profile, which is mainly determined by the long prepulse. During the main pumping pulse, the electron density has little change. The x-ray laser is expected to be amplified at the region with electron density between $4-8 \times 10^{19}$ cm^{-3} and 1.2×10^{20} cm^{-3}.

The parameters of the main pulse are also optimized following the optimization of the prepulse and delay conditions. Figure 8(a) shows the gain contours produced by the main pulse of 1 ps with a peak intensity of 2×10^{14} W/cm^2. The color from the light to the dark represents the gain over 50, 70, and 100 cm^{-1}, respectively. The highest local gain is over 150 cm^{-1} in several micrometers of the effective absorption region and only maintains several picoseconds. Figure 8(b) shows the profile of spatially integrated laser output intensity as a function of the plasma length with the refraction and saturation effects taken into account under the optimized pumping configuration. The x-ray lasers operate in the saturation regime with a target longer than 0.3 cm and the gain-length product around 15. The effective gain coefficient is 58.7 cm^{-1}. Based on the above analysis, we predict that the saturation operation of the x-ray laser at 14.7 nm can be realized using the optimized driving pulse configuration with only subjoule energy.

V. CONCLUSION

In summary, MEDUSA was modified for the research of the grazing-incidence pumping scheme of x-ray lasers. The operation of the Ni-like Pd x-ray laser at 14.7 nm ($4d \rightarrow 4p$, $J=0 \rightarrow 1$) pumped by such a scheme is investigated. The grazing incidence angle of the main short pulse is optimized to be 14.5°. The effective gain coefficient is 58.7 cm^{-1}. The results predict that saturation operation of the x-ray laser at 14.7 nm can be achieved with only several hundreds of millijoules on a 4 mm slab target. Using the optimized parameters, an experiment is designed and to be conducted soon using the XL-II laser system.

[1] D. L. Matthews *et al.*, Phys. Rev. Lett. **54**, 110 (1984).

[2] M. D. Rosen in *OSA Proceedings on Short Wavelength Coherent Radiation: Generation and Applications*, edited by Philip H. Buchsbaum and Natale M. Ceglio (Optical Society of America, Washington, D.C., 1991), Vol. 11, p. 73; L. Da Silva *et al.* Proc. SPIE **1229**, 128 (1990).

[3] J. Nilsen and J. C. Moreno, Phys. Rev. Lett. **74**, 3376 (1995).

[4] J. Zhang *et al.*, Phys. Rev. Lett. **78**, 3856 (1997).

[5] J. Zhang *et al.*, Science **276**, 1097 (1997).

[6] P. V. Nickles, V. N. Shlyaptsev, M. Kalachynikov, M. Schnürer, I. Will, and W. Sandner, Phys. Rev. Lett. **78**, 2748 (1997).

[7] Yu. V. Afanasiev and V. N. Shlyaptsev, Sov. J. Quantum Electron. **19**, 1606 (1989).

[8] B. Rus, T. Mocek, A. R. Präg, M. Kozlová, G. Jamelot, A. Carillon, D. Ros, D. Joyeux, and P. Phalippou, Phys. Rev. A **66**, 063806 (2002).

[9] J. Y. Lin *et al.*, Opt. Commun. **166**, 211 (1999).

[10] T. Kawachi *et al.*, Phys. Rev. A **66**, 033815 (2002).

[11] J. Dunn, Y. Li, A. L. Osterheld, J. Nilsen, J. R. Hunter, and V. N. Shlyaptsev, Phys. Rev. Lett. **84**, 4834 (2000).

[12] R. Tommasini *et al.*, J. Opt. Soc. Am. B **16**, 1664 (1999).

[13] S. Sebban *et al.*, Phys. Rev. A **61**, 043810 (2000).

[14] T. Kawachi *et al.*, Phys. Rev. A **66**, 033815 (2002).

[15] K. A. Janulewicz, A. Lucianetti, G. Priebe, W. Sandner, and P. V. Nickles, Phys. Rev. A **68**, 051802(R) (2003).

[16] T. Ozaki, R. A. Ganeev, A. Ishizawa, T. Kanai, and H. Kuroda, Phys. Rev. Lett. **89**, 253902 (2002).

[17] J. Dunn *et al.* in *X-Ray Lasers 2004: Proceedings of the 9th International Conference on X-Ray Lasers*, edited by Jie Zhang, (Institute of Physics Publishing, Bristol and Philadelphia, 2004), IoP Inst. Phys. Conf. Ser. No 186, p. 305.

[18] R. Keenan, J. Dunn, P. K. Patel, D. F. Price, R. F. Smith, and V. N. Shlyaptsev, Phys. Rev. Lett. **94**, 103901 (2005).

[19] J. Dunn (private communication).

[20] J. P. Christiansen, D. Ashby, and K. V. Roberts, Chem. Phys. **7**, 271 (1974).

[21] J. Tummler, K. A. Janulevicz, G. Priebe, and P. V. Nickles, Phys. Rev. E **72**, 037401 (2005).

[22] B. M. Luther *et al.*, Opt. Lett. **30**, 165 (2005).

[23] H. Daido *et al.*, Int. J. Mod. Phys. B **11**, 945 (1996).